PERGAMON

International Journal of Solids and Structures 37 (2000) 6479–6497

INTERNATIONAL JOURNAL OF SOLIDS and STRUCTURES

www.elsevier.com/locate/ijsolstr

A higher order temperature theory for coupled thermo-piezoelectric-mechanical modeling of smart composites

Haozhong Gu, Aditi Chattopadhyay*, Jingmei Li, Xu Zhou

Department of Mechanical and Aerospace Engineering, Arizona State University, Tempe, AZ 85287-6106, USA

Received 15 January 1999; in revised form 11 June 1999

Abstract

A higher order temperature field that satisfies the thermal surface boundary conditions, necessary for accurate modeling of temperature distribution through the thickness of laminated structures, is developed. The theory is implemented in the coupled thermo-piezoelectric-mechanical analysis of composite laminates with surface bonded piezoelectric actuators. A higher order displacement theory is used to define the mechanical displacement field. Therefore, transverse shear effects are modeled accurately and the developed procedure is applicable to both thin and moderately thick laminates. The mathematical model is implemented using finite element technique. Numerical results are presented for a composite laminated plate, with one edge fixed, subjected to thermal loading. Correlations with ANSYS, for both the temperature field and the displacement field, are presented to validate the higher order temperature theory. Composite laminates of various stacking sequences are studied to investigate the effects on temperature field and displacement field. The results obtained using the coupled theory are compared with those obtained using the standard uncoupled theory. It is shown that thermal coupling affects plate deflection and control authority due to actuation. © 2000 Elsevier Science Ltd. All rights reserved.

Keywords: Laminate; Temperature; Piezoelectric; Coupling

1. Introduction

The development of smart composites offers great potential for use in advanced aerospace structures because they are light in weight and possess adaptive control capabilities. Detailed overviews of the current status of smart composite structures were reported by Crawley (1994) and Chopra (1996). For the analysis of these structures, it is essential to accurately model both the strain field and the electric

* Corresponding author. Tel.: +1-480-965-9342; fax: +1-480-965-1384.
E-mail address: aditi@asu.edu (A. Chattopadhyay).

0020-7683/00/$ - see front matter © 2000 Elsevier Science Ltd. All rights reserved.
PII: S0020-7683(99)00283-8

Nomenclature

$\mathbf{B}_u$, $\mathbf{B}_\phi$, $\mathbf{B}_\theta$	operator matrices
b_{ij}	dielectric permittivity, $i, j = 1, 2, 3$
c_E	heat capacity
c_{ijkl}	elastic constants, $i, j, k, l = 1, 2, 3$
D_i	electric displacement components, $i = 1, 2, 3$
d_i	thermal-piezoelectric coupling constants, $i = 1, 2, 3$
E_i	electric field components, $i = 1, 2, 3$
e_{ijk}	piezoelectric constants, $i, j, k = 1, 2, 3$
F	total free energy
H	plate thickness including piezoelectric layers
h	plate thickness without piezoelectric layers
k_{ij}	thermal-mechanical coupling constants, $i, j = 1, 2, 3$
$\mathbf{L}_1$, $\mathbf{L}_2$, $\mathbf{L}_3$	operator matrices
$\mathbf{N}_1$, $\mathbf{N}_2$, $\mathbf{N}_3$	interpolation matrices
q_e	charge density
q_s	heat flux density
S	entropy
T_0	initial temperature
t_i	traction, $i = 1, 2, 3$
u_i	displacement components, $i = 1, 2, 3$
u_0, v_0, w_0	displacements of a point on the mid plane
V	volume
x, y, z	coordinates
α_T	material constant ($\alpha_T = c_E/T_0$)
ε_{ij}	strain tensor components, $i, j = 1, 2, 3$
θ	temperature rise from initial temperature (T_0)
κ_{ij}	thermal conductivity, $i, j = 1, 2, 3$
α_{ij}	stress tensor components, $i, j = 1, 2, 3$
ϕ	electric potential
$()^{\mathrm{T}}$	transpose

field. However, most studies in smart structures considered only one-way interaction between the mechanical field and the piezoelectric field. For example, in the analysis of a structure with actuators, it is assumed that the piezoelectric field can be calculated directly from applied voltage, which is then introduced in the unknown displacement field as an induced strain. Actually, not only does piezoelectric actuation change the strain field during active control of the structure, the new strain field, in return, affects the piezoelectric distributions. This is known as bi-way interaction in smart composites (Mitchell and Reddy, 1995).

In addition, aerospace smart structures are often subjected to extensive thermal loads. Therefore, it is necessary to accurately model the temperature distribution and the associated coupling effects. A better understanding of bi-way coupling effects between temperature, piezoelectric and mechanical fields is essential for the proper implementation of smart composites and active control techniques in the presence of thermal loads. Unfortunately, limited research has been reported in this area. In Tauchert (1992), one-way thermal-mechanical and one-way thermal-piezoelectric coupling effects based on the

classical laminated theory were addressed. A layerwise theory was used to model smart composite plates under thermal loads using a known thermal field (Lee and Saravanos, 1996, Lee and Saravanos, 1997). Again, the bi-way coupling effects between thermal-piezoelectric and thermal-mechanical responses were ignored. Recently, a coupled thermo-piezoelectric-mechanical model was developed by Chattopadhyay et al. to address the bi-way coupling issues associated with smart composites under thermal loads (Chattopadhyay et al, 1998). However, a linear temperature field, which is generally used in plate problems to define the temperature variation through the plate thickness, was used. The advantage of the linear temperature field is that it is easy to implement. However, the drawback is that it cannot accurately satisfy thermal boundary conditions on the plate surfaces. Even for the numerical example considered by Chattopadhyay et al. (1998), the heat flux boundary conditions at the plate top surface and the insulated boundary conditions at the plate bottom surface were not satisfied. Therefore, the use of a linear temperature field does not provide an accurate representation of the temperature distribution through the laminate thickness. Consequently, the plate out-of-plane bending moment, due to thermal loads, is not modeled accurately. To address this issue, a new higher order temperature (HOT) field is developed in this paper for accurately modeling the temperature field through the plate thickness. The developed temperature field satisfies the general thermal boundary conditions at both the top and bottom surfaces of the laminates. It must be noted that although this theory is developed to study smart structures, it can be widely used in the analysis of arbitrary plate structures. Also by Chattopadhyay et al. (1998), the Rayleigh approach was used in the numerical implementation of the coupled theory. This limits the application of the theory to practical structures and boundary conditions. In this paper, a finite element procedure is developed to implement the coupled thermo-piezoelectric-mechanical theory. Therefore, the procedure is capable of addressing different laminate geometry and boundary conditions.

2. Mathematical formulation

The governing equations are derived by applying the principle of free energy and the variational principle. For the plate shown in Fig. 1, the total free energy of the structure can be written as

$$F(\varepsilon_{ij}, E_i, \theta) = \frac{1}{2}c_{ijkl}\varepsilon_{ij}\varepsilon_{kl} - e_{ijk}E_i\varepsilon_{jk} - \frac{1}{2}b_{ij}E_iE_j - k_{ij}\theta\varepsilon_{ij} - d_iE_i\theta - \frac{1}{2}a_T\theta^2 \tag{1}$$

where ε_{ij} are the components of the strain tensor, E_i are the components of the electric field vector, and θ is the temperature rise from the initial temperature T_0. The quantities c_{ijkl} and e_{ijk} represent the elastic and the piezoelectric constants, respectively and b_{ij} is the dielectric permittivity. The quantities k_{ij} and d_i refer to the thermal-mechanical, and the thermal-piezoelectric coupling constants, respectively and a_T is defined as c_E/T_0, where c_E is heat capacity. Consequently, the constitutive relations are

$$\sigma_{ij} = \frac{\partial F}{\partial \varepsilon_{ij}} = c_{ijkl}\varepsilon_{kl} - e_{ijk}E_k - k_{ij}\theta \tag{2}$$

$$D_i = -\frac{\partial F}{\partial E_i} = e_{ijk}\varepsilon_{jk} + b_{ij}E_j + d_i\theta \tag{3}$$

$$S = -\frac{\partial F}{\partial \theta} = k_{ij}\varepsilon_{ij} + d_iE_i + a_T\theta \tag{4}$$

where σ_{ij} and D_i are the components of the stress tensor and the electric displacement vector,

respectively and S is the entropy. Based on linear piezoelectricity, E_i is derivable from a scalar potential function ϕ as follows:

$$E_i = -\phi_{,i} \quad (i = 1, 2, 3) \tag{5}$$

The governing equations are now derived using variational principle, assuming no body force, as follows:

$$0 = -\int_0^{t_0}\int_V \sigma_{ij}\delta\varepsilon_{ij}\mathrm{d}V\,\mathrm{d}t + \int_0^{t_0}\int_S t_i\delta u_i\mathrm{d}S\,\mathrm{d}t = \delta U + \delta F_1 \tag{6}$$

$$0 = -\int_0^{t_0}\int_V D_i\delta\phi_{,i}\mathrm{d}V\,\mathrm{d}t + \int_0^{t_0}\int_S q_e\delta\phi\mathrm{d}S\,\mathrm{d}t = \delta E + \delta F_2 \tag{7}$$

$$0 = \int_0^{t_0}\int_V \left[\kappa_{ij}\theta_{,i}\delta\theta_{,j} + \dot{S}T_0\delta\theta\right]\mathrm{d}V\,\mathrm{d}t + \int_0^{t_0}\int_S q_s\delta\theta\mathrm{d}S\,\mathrm{d}t = \delta\Theta_k + \delta\Theta_c + \delta F_3 \tag{8}$$

In Eqs. (6)–(8), κ_{ij} denotes the thermal conductivity, $\dot{S}$ denotes the derivative of S with respect to time, t_i represents the components of the traction vector, q_e and q_s represent the charge density and heat flux, respectively. It must be noted that Eqs. (6)–(8) address temperature, piezoelectric and mechanical fields

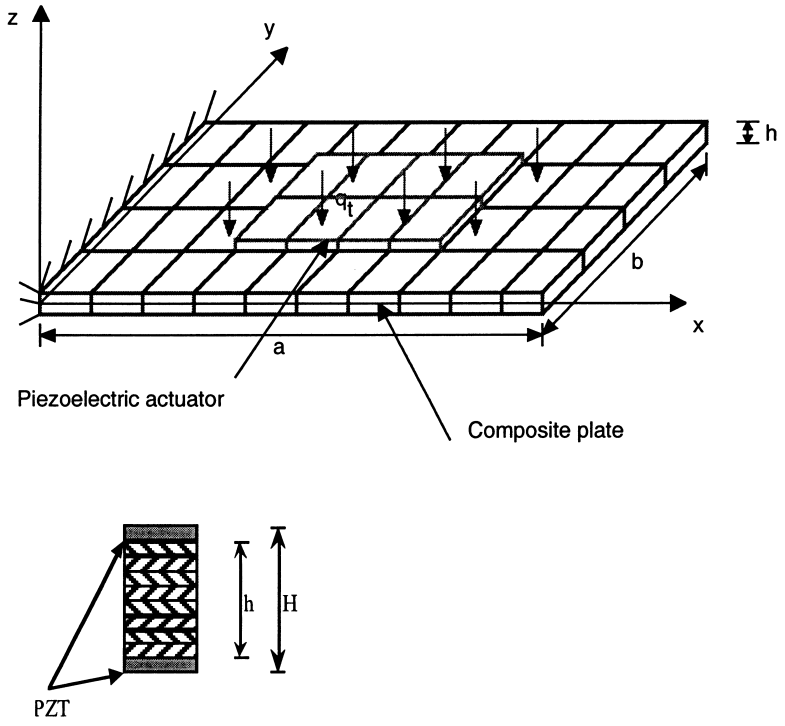

Fig. 1. Geometry of composite laminate with piezoelectric layers.

simultaneously and represent the governing equations of the coupled thermo-piezoelectric-mechanical theory.

2.1. Higher order displacement field

The present theory uses a displacement approach. The displacement field is assumed according to the higher order displacement theory, which incorporates the transverse shear effects. The form is dictated by the satisfaction of the conditions that the transverse shear stresses vanish on the plate surfaces and be nonzero values elsewhere. The higher order displacement field can be written as

$$u_1(x, y, z, t) = u_0(x, y, t) - z\frac{\partial w_0(x,y,t)}{\partial x} + g(z)\psi_x(x, y, t) \tag{9}$$

$$u_2(x, y, z, t) = v_0(x, y, t) - z\frac{\partial w_0(x, y, t)}{\partial y} + g(z)\psi_y(x, y, t) \tag{10}$$

$$u_3(x, y, z, t) = w_0(x, y, t) \tag{11}$$

with

$$g(z) = z - \frac{4}{3H^2}z^3 \tag{12}$$

In Eqs. (9)–(11), u_0, v_0 and w_0 are the displacements of a point in the middle plane of the laminate, ψ_x and ψ_y are the rotations of a transverse normal at $z = 0$ about the y and -x axes, respectively and H indicates the total thickness of the plate including the piezoelectric layers (Fig. 1).

2.2. Layerwise linear piezoelectric field

The expression for the potential function (ϕ) is assumed to be layerwise and linear along z-axis in each layer

$$\phi^j(x, y, z, t) = \phi_0^j(x, y, t) + z\phi_1^j(x, y, t) \quad (j = 1, 2) \tag{13}$$

where j indicates the layer of piezoelectric laminae. Because only top and bottom surface bonded piezoelectric actuators are studied in this work, $j = 1$ indicates the piezoelectric layer at bottom and $j = 2$ indicates the piezoelectric layer on top.

2.3. Higher order temperature field

In the higher order temperature theory, temperature field (θ) is assumed as a cubic function of the thickness of the plate, z.

$$\theta(x, y, z, t) = \theta_0(x, y, t) + z\theta_1(x, y, t) + z^2\theta_2(x, y, t) + z^3\theta_3(x, y, t) \tag{14}$$

In general, the plate may be subjected to thermal loads at both top and bottom surfaces, so that the two thermal boundary conditions on both surfaces expressed as

$$-\kappa_{33}\theta_{,z} = q_t \quad z = H/2 \tag{15}$$

$$-\kappa_{33}\theta_{,z} = q_b \quad z = -H/2 \tag{16}$$

should be satisfied. Where q_t and q_b indicate the heat flux applied on top and bottom surfaces, respectively. Whereas, κ_{33} denotes the thermal conductivity through the thickness. The two higher order terms in Eq. (14) can be identified in terms of the lower order terms, using the boundary conditions defined in Eqs. (15) and (16), as follows:

$$\theta(x, y, z, t) = f(z) + \theta_0(x, y, t) + g(z)\theta_1(x, y, t) \tag{17}$$

where the function $g(z)$ has been defined in Eq. (12) and the function $f(z)$ takes the following form:

$$f(z) = -\frac{z^2}{2H}\frac{q_t - q_b}{\kappa_{33}} - \frac{2z^3}{3H^2}\frac{q_t + q_b}{\kappa_{33}}$$

It must be noted that the higher order temperature field defines a nonuniform temperature distribution in the plate (both in- and out-of-plane). The cubic functions $f(z)$ and $g(z)$ in Eq. (17), which are developed for a two-dimensional element and are calculated from the thermal boundary conditions on the surfaces, denote temperature variations through the plate thickness. The functions $\theta_0(x, y)$ and $\theta_1(x, y)$ define the in-plane temperature variations and are calculated using finite element method and thermal boundary conditions along the plate sides. It is important to note that although a linear temperature filed can address the in-plane temperature distribution, it cannot satisfy the surface thermal boundary conditions defined in Eqs. (15) and (16). Therefore, temperature variations through the thickness, which produce the most important bending deformation, cannot be modeled accurately by the linear temperature field.

3. Finite element model and solution

Using Eqs. (9)–(11), the strain vector can be written as follows:

$$\boldsymbol{\varepsilon} = \begin{bmatrix} \varepsilon_1 \\ \varepsilon_2 \\ \varepsilon_4 \\ \varepsilon_5 \\ \varepsilon_6 \end{bmatrix} = \begin{bmatrix} \dfrac{\partial u_1}{\partial x} \\ \dfrac{\partial u_2}{\partial y} \\ \dfrac{\partial u_2}{\partial z} + \dfrac{\partial u_3}{\partial y} \\ \dfrac{\partial u_1}{\partial z} + \dfrac{\partial u_3}{\partial x} \\ \dfrac{\partial u_1}{\partial y} + \dfrac{\partial u_2}{\partial x} \end{bmatrix} = \begin{bmatrix} \dfrac{\partial}{\partial x} & 0 & -z\dfrac{\partial^2}{\partial x^2} & g(z)\dfrac{\partial}{\partial x} & 0 \\ 0 & \dfrac{\partial}{\partial y} & -z\dfrac{\partial^2}{\partial^2 y} & 0 & g(z)\dfrac{\partial}{\partial y} \\ 0 & 0 & 0 & 0 & \dfrac{dg(z)}{dz} \\ 0 & 0 & 0 & \dfrac{dg(z)}{dz} & 0 \\ \dfrac{\partial}{\partial y} & \dfrac{\partial}{\partial x} & -2z\dfrac{\partial^2}{\partial x \partial y} & g(z)\dfrac{\partial}{\partial y} & g(z)\dfrac{\partial}{\partial x} \end{bmatrix} \begin{bmatrix} u_0 \\ v_0 \\ w_0 \\ \psi_x \\ \psi_y \end{bmatrix} = \mathbf{L}_1 \mathbf{u}_u \tag{18}$$

In Eq. (18), the matrix $\mathbf{L}_1$ is an operator matrix and $\mathbf{u}_u = [u_0 \quad v_0 \quad w_0 \quad \psi_x \quad \psi_y]^T$.

The expressions for the electric field (E^j) and the temperature field (θ) can be derived as follows:

$$\mathbf{E}^{j} = -\begin{Bmatrix} \dfrac{\partial \phi^{j}}{\partial x} \\ \dfrac{\partial \phi^{j}}{\partial y} \\ \dfrac{\partial \phi^{j}}{\partial z} \end{Bmatrix} = -\begin{bmatrix} \dfrac{\partial}{\partial x} & z\dfrac{\partial}{\partial x} \\ \dfrac{\partial}{\partial y} & z\dfrac{\partial}{\partial y} \\ 0 & 1 \end{bmatrix} \begin{Bmatrix} \phi_0^{j} \\ \phi_1^{j} \end{Bmatrix} = \mathbf{L}_2 \mathbf{u}_{\phi}^{j} \quad (j = 1, 2) \tag{19}$$

$$\theta = f(z) + \theta_0 + g(z)\theta_1 = f(z) + \mathbf{L}_3 \mathbf{u}_{\theta} \tag{20}$$

where $\mathbf{L}_2$ and $\mathbf{L}_3$ are piezoelectric and thermal operator matrices, respectively and $\mathbf{u}_{\phi}^{j} = [\,\phi_0^{j} \quad \phi_1^{j}\,]^T$ indicates the potential variable vector for the jth layer of piezoelectric laminae. Thermal variable vector is expressed as $\boldsymbol{u}_{\theta} = [\,\theta_0 \quad \theta_1\,]^T$.

Considering a rectangular plate finite element with four nodes, bilinear Lagrangian interpolation functions (N_i, $i = 1, 2, 3, 4$) are used for u_0, v_0, ψ_x and ψ_y and Hermite interpolation functions (H_{1i}, H_{2i}, and H_{3i}, $i = 1, 2, 3, 4$) are used for w_0. Hence, the displacement vector $\mathbf{u}_u$ can be expressed as follows:

$$\mathbf{u}_u = \mathbf{N}_1 \mathbf{u}_u^e \tag{21}$$

where

$$\mathbf{N}_1 = \begin{bmatrix} \mathbf{N}_1^{(1)} & \mathbf{N}_1^{(2)} & \mathbf{N}_1^{(3)} & \mathbf{N}_1^{(4)} \end{bmatrix} \quad \text{and} \quad \mathbf{u}_u^e = \begin{bmatrix} \mathbf{u}_u^{e(1)} & \mathbf{u}_u^{e(2)} & \mathbf{u}_u^{e(3)} & \mathbf{u}_u^{e(4)} \end{bmatrix}^{\mathrm{T}}$$

with

$$\mathbf{N}_1^{(i)} = \begin{bmatrix} N_i & 0 & 0 & 0 & 0 & 0 & 0 \\ 0 & N_i & 0 & 0 & 0 & 0 & 0 \\ 0 & 0 & H_{1i} & H_{2i} & H_{3i} & 0 & 0 \\ 0 & 0 & 0 & 0 & 0 & N_i & 0 \\ 0 & 0 & 0 & 0 & 0 & 0 & N_i \end{bmatrix} \quad (i = 1, 2, 3, 4)$$

and

$$\mathbf{u}_u^{e(i)} = \begin{bmatrix} u_0^i & v_0^i & w_0^i & w_{0,x}^i & w_{0,y}^i & \psi_x^i & \psi_y^i \end{bmatrix}^{\mathrm{T}} \quad (i = 1, 2, 3, 4)$$

where $\mathbf{N}_1$ indicates the interpolation matrix, $\mathbf{u}_u^e$ denotes a vector containing the displacement variables on the four nodes. By using Eqs. (18) and (21), the strain vector can be expressed as follows:

$$\boldsymbol{\varepsilon} = \mathbf{B}_u \mathbf{u}_u^e \tag{22}$$

where

$$\mathbf{B}_u = \begin{bmatrix} \mathbf{B}_u^{(1)} & \mathbf{B}_u^{(2)} & \mathbf{B}_u^{(3)} & \mathbf{B}_u^{(4)} \end{bmatrix}$$

with

$$\mathbf{B}_u^{(i)} = \begin{bmatrix} \frac{\partial N_i}{\partial x} & 0 & -z\frac{\partial^2 H_{1i}}{\partial x^2} & -z\frac{\partial^2 H_{2i}}{\partial x^2} & -z\frac{\partial^2 H_{3i}}{\partial x^2} & g(z)\frac{\partial N_i}{\partial x} & 0 \\ 0 & \frac{\partial N_i}{\partial y} & -z\frac{\partial^2 H_{1i}}{\partial y^2} & -z\frac{\partial^2 H_{2i}}{\partial y^2} & -z\frac{\partial^2 H_{3i}}{\partial y^2} & 0 & g(z)\frac{\partial N_i}{\partial y} \\ 0 & 0 & 0 & 0 & 0 & 0 & \frac{dg(z)}{dz}N_i \\ 0 & 0 & 0 & 0 & 0 & \frac{dg(z)}{dz}N_i & 0 \\ \frac{\partial N_i}{\partial y} & \frac{\partial N_i}{\partial x} & -2z\frac{\partial^2 H_{1i}}{\partial x \partial y} & -2z\frac{\partial^2 H_{1i}}{\partial x \partial y} & -2z\frac{\partial^2 H_{1i}}{\partial x \partial y} & g(z)\frac{\partial N_i}{\partial y} & g(z)\frac{\partial N_i}{\partial x} \end{bmatrix}$$

Again, using bilinear Lagrangian interpolation functions for ϕ_0 and ϕ_1, the vector $\mathbf{u}_\phi$ is expressed as

$$\mathbf{u}_\phi = \mathbf{N}_2 \mathbf{u}_\phi^e \tag{23}$$

where

$$\mathbf{N}_2 = \begin{bmatrix} \mathbf{N}_2^{(1)} & \mathbf{N}_2^{(2)} & \mathbf{N}_2^{(3)} & \mathbf{N}_2^{(4)} \end{bmatrix} \quad \text{and} \quad \mathbf{u}_\phi^e = \begin{bmatrix} \mathbf{u}_\phi^{e(1)} & \mathbf{u}_\phi^{e(2)} & \mathbf{u}_\phi^{e(3)} & \mathbf{u}_\phi^{e(4)} \end{bmatrix}^{\mathrm{T}}$$

with

$$\mathbf{N}_2^{(i)} = \begin{bmatrix} N_i & 0 \\ 0 & N_i \end{bmatrix} \quad (i = 1, 2, 3, 4)$$

and

$$\mathbf{u}_\phi^{e(i)} = \begin{bmatrix} \phi_0^i & \phi_1^i \end{bmatrix}^{\mathrm{T}} \quad (i = 1, 2, 3, 4)$$

where $\mathbf{N}_2$ is an interpolation matrix, $\boldsymbol{u}_\phi^e$ denotes the potential variables on four nodes for each element. From Eqs. (19) and (23), the electric field ($\mathbf{E}$) is expressed as

$$\mathbf{E} = \mathbf{B}_\phi \mathbf{u}_\phi^e \tag{24}$$

where

$$\mathbf{B}_\phi = \begin{bmatrix} \mathbf{B}_\phi^{(1)} & \mathbf{B}_\phi^{(2)} & \mathbf{B}_\phi^{(3)} & \mathbf{B}_\phi^{(4)} \end{bmatrix}$$

with

$$\mathbf{B}_\phi^{(i)} = \begin{bmatrix} \frac{\partial N_i}{\partial x} & z\frac{\partial N_i}{\partial x} \\ \frac{\partial N_i}{\partial y} & z\frac{\partial N_i}{\partial y} \\ 0 & N_i \end{bmatrix} \quad (i = 1, 2, 3, 4)$$

Once again, Lagrangian interpolation functions are used to interpolate the thermal variables. $\mathbf{u}_\theta$ is defined as

$$\mathbf{u}_\theta = \mathbf{N}_3 \mathbf{u}_\theta^e \tag{25}$$

where

$$\mathbf{N}_3 = \begin{bmatrix} \mathbf{N}_3^{(1)} & \mathbf{N}_3^{(2)} & \mathbf{N}_3^{(3)} & \mathbf{N}_3^{(4)} \end{bmatrix} \quad \text{and} \quad \mathbf{u}_\theta^e = \begin{bmatrix} \mathbf{u}_\theta^{e^{(1)}} & \mathbf{u}_\theta^{e^{(2)}} & \mathbf{u}_\theta^{e^{(3)}} & \mathbf{u}_\theta^{e^{(4)}} \end{bmatrix}^{\mathrm{T}}$$

with

$$\mathbf{N}_3^{(i)} = \begin{bmatrix} N_i & 0 \\ 0 & N_i \end{bmatrix} \quad (i = 1, 2, 3, 4)$$

and

$$\mathbf{u}_\theta^{e^{(i)}} = \begin{bmatrix} \theta_0^i & \theta_1^i \end{bmatrix}^{\mathrm{T}} \quad (i = 1, 2, 3, 4)$$

where $\mathbf{N}_3$ indicates an interpolation matrix, $\mathbf{u}_\theta^e$ denotes vectors containing the nodal values on the four nodes. Thus, the temperature field vector takes the following form:

$$\theta = f(z) + \mathbf{B}_\theta \mathbf{u}_\theta^e \tag{26}$$

where

$$\mathbf{B}_\theta = \begin{bmatrix} \mathbf{B}_\theta^{(1)} & \mathbf{B}_\theta^{(2)} & \mathbf{B}_\theta^{(3)} & \mathbf{B}_\theta^{(4)} \end{bmatrix}$$

with

$$\mathbf{B}_\theta^{(i)} = \begin{bmatrix} N_i & g(z)N_i \end{bmatrix} \quad (i = 1, 2, 3, 4)$$

Rewrite Eqs. (2)–(4) in vector form, they are

$$\boldsymbol{\sigma} = \mathbf{Q}\boldsymbol{\varepsilon} - \mathbf{P}\mathbf{E} - \mathbf{k}\theta \tag{27}$$

$$\mathbf{D} = \mathbf{P}^{\mathrm{T}}\boldsymbol{\varepsilon} + \boldsymbol{\beta}\mathbf{E} + \mathbf{d}\theta \tag{28}$$

$$S = \mathbf{k}^{\mathrm{T}}\varepsilon + \mathbf{d}^{\mathrm{T}}\mathbf{E} + a_T\theta \tag{29}$$

where $\boldsymbol{\sigma}$ and $\mathbf{D}$ are the stress vector and the electric displacement vector, respectively and $\boldsymbol{\varepsilon}$ and $\mathbf{E}$ are the strain vector and the electric field vector, respectively. Matrices $\mathbf{Q}$, $\mathbf{B}$, $\mathbf{P}$, $\mathbf{k}$ and $\mathbf{d}$ denote the matrix forms of elastic constant, dielectric permittivity, piezoelectric constant, thermal-mechanical coupling constant and thermal-piezoelectric coupling constant, respectively. The use of Eqs. (27)–(29), (22), (24) and (26) in Eqs. (6)–(8) and integration with respect to volume V yields the following:

$$\begin{aligned} \delta U &= -\int_0^{t_0}\int_V \delta\boldsymbol{\varepsilon}^{\mathrm{T}}\boldsymbol{\sigma}\,\mathrm{d}V\,\mathrm{d}t = -\int_0^{t_0}\int_V \delta\boldsymbol{\varepsilon}^{\mathrm{T}}(\mathbf{Q}\boldsymbol{\varepsilon} - \mathbf{P}\mathbf{E} - \mathbf{k}\theta)\mathrm{d}V\,\mathrm{d}t \\ &= -\int_0^{t_0}\int_V \delta\mathbf{u}_u^{e^T}\mathbf{B}_u^T\left(\mathbf{Q}\mathbf{B}_u\mathbf{u}_u^e - \mathbf{P}\mathbf{B}_\phi\mathbf{u}_\phi^e - \mathbf{k}\mathbf{B}_\theta\mathbf{u}_\theta^e\right)\mathrm{d}V\,\mathrm{d}t + \int_0^{t_0}\int_V \delta\mathbf{u}_u^{e^T}\mathbf{B}_u^T f(z)\mathrm{d}V\,\mathrm{d}t \\ &= \delta\mathbf{u}_u^{e^T}\int_0^{t_0}\left(\mathbf{K}_{uu}\mathbf{u}_u^e + \mathbf{K}_{u\phi}\mathbf{u}_\phi^e + \mathbf{K}_{u\theta}\mathbf{u}_\theta^e + \mathbf{F}_{u\theta}\right)\mathrm{d}t \end{aligned} \tag{30}$$

$$\delta E = \int_0^{t_0}\int_V \delta \mathbf{E}^{\mathrm{T}}\mathbf{D}dV\,\mathrm{d}t = \int_0^{t_0}\int_V \delta\mathbf{E}^{\mathrm{T}}\left(\mathbf{P}^{\mathrm{T}}\boldsymbol{\varepsilon} + \boldsymbol{\beta}\mathbf{E} + \mathbf{d}\theta\right)\mathrm{d}V\,\mathrm{d}t$$

$$= -\int_0^{t_0}\int_V \delta\mathbf{u}_\phi^{e^T}\mathbf{B}_\phi^T\left(\mathbf{P}\mathbf{B}_u\mathbf{u}_u^e - \boldsymbol{\beta}\mathbf{B}_\phi\mathbf{u}_\phi^e - \mathbf{d}\mathbf{B}_\theta\mathbf{u}_\theta^e\right)\mathrm{d}V\,\mathrm{d}t + \int_0^{t_0}\int_V \delta\mathbf{u}_\phi^{e^T}\mathbf{B}_\phi^T f(z)\mathrm{d}V\,\mathrm{d}t$$

$$= \delta\mathbf{u}_\phi^{e^T}\int_0^{t_0}\left(\mathbf{K}_{\phi u}\mathbf{u}_u^e + \mathbf{K}_{\phi\phi}\mathbf{u}_\phi^e + \mathbf{K}_{\phi\theta}\mathbf{u}_\theta^e + \mathbf{F}_{\phi\theta}\right)\mathrm{d}t \tag{31}$$

$$\delta\Theta_k = \int_0^{t_0}\int_V \kappa_{ij}\theta_{,i}\delta\theta_{,j}\mathrm{d}V\,\mathrm{d}t = \int_0^{t_0}\int_V \delta\theta\mathbf{L}_4^T\boldsymbol{\kappa}\mathbf{L}_4\theta\mathrm{d}V\,\mathrm{d}t = \int_0^{t_0}\int_V \delta\mathbf{u}_\theta^{e^T}\mathbf{B}_t^T\boldsymbol{\kappa}\mathbf{B}_t\mathbf{u}_\theta^e\mathrm{d}V\,\mathrm{d}t$$

$$= \delta\mathbf{u}_\theta^{e^T}\int_0^{t_0}\mathbf{K}_{\theta\theta}\mathbf{u}_\theta^e\,\mathrm{d}t \tag{32}$$

$$\delta\Theta_c = \int_0^{t_0}\int_V \dot{S}T_0\delta\theta\mathrm{d}V\,\mathrm{d}t = \int_0^{t_0}\int_V T_0\delta\theta\left(\mathbf{k}^T\dot{\varepsilon} + \mathbf{d}^T\dot{\mathbf{E}} + a_T\dot{\theta}\right)\mathrm{d}V\,\mathrm{d}t$$

$$= T_0\int_0^{t_0}\int_V \delta\mathbf{u}_\theta^{e^T}\mathbf{B}_\theta^T\left(\mathbf{k}^T\mathbf{B}_\theta\dot{\mathbf{u}}_u^e + \mathbf{d}^T\mathbf{B}_\theta\dot{\mathbf{u}}_\phi^e + a_T\mathbf{B}_\theta\dot{\mathbf{u}}_\theta^e\right)\mathrm{d}V\,\mathrm{d}t$$

$$= \delta\mathbf{u}_\theta^{e^T}\int_0^{t_0}\left(\mathbf{C}_{\theta u}\dot{\mathbf{u}}_u^e + \mathbf{C}_{\theta\phi}\dot{\mathbf{u}}_\phi^e + \mathbf{C}_{\theta\theta}\dot{\mathbf{u}}_\theta^e\right)\mathrm{d}t \tag{33}$$

The variation involving the force terms can be written as follows:

$$\delta F_1 = \int_0^{t_0}\int_S \delta\mathbf{u}^{\mathrm{T}}\mathbf{t}dS\,\mathrm{d}t = \int_0^{t_0}\int_S \delta\mathbf{u}_u^{e^T}\mathbf{B}_m^T\mathbf{t}dS\,\mathrm{d}t = \delta\mathbf{u}_u^{e^T}\int_0^{t_0}\mathbf{F}_u\,\mathrm{d}t \tag{34}$$

$$\delta F_2 = \int_0^{t_0}\int_S \delta\phi q_e\mathrm{d}S\,\mathrm{d}t = \int_0^{t_0}\int_S \delta\mathbf{u}_\phi^{e^T}\mathbf{B}_p^T q_e\mathrm{d}S\,\mathrm{d}t = \delta\mathbf{u}_\phi^{e^T}\int_0^{t_0}\mathbf{F}_\phi\,\mathrm{d}t \tag{35}$$

$$\delta F_3 = \int_0^{t_0}\int_S \delta\theta q_t\mathrm{d}S\,\mathrm{d}t = \int_0^{t_0}\int_S \delta u_\theta^{e^T}\mathbf{B}_\theta^T q_t\mathrm{d}S\,\mathrm{d}t = \delta\mathbf{u}_\theta^{e^T}\int_0^{t_0}\mathbf{F}_\theta\,\mathrm{d}t \tag{36}$$

Substituting Eqs. (30)–(36) into Eqs. (6)–(8), the following finite element governing equations of the thermo-piezoelectric-mechanical coupled theory, based on the higher order temperature field, are obtained.

$$\begin{bmatrix} 0 & 0 & 0 \\ 0 & 0 & 0 \\ \mathbf{C}_{\theta u} & \mathbf{C}_{\theta\phi} & \mathbf{C}_{\theta\theta} \end{bmatrix}\begin{Bmatrix} \dot{\mathbf{u}}_u^e \\ \dot{\mathbf{u}}_\phi^e \\ \dot{\mathbf{u}}_\theta^e \end{Bmatrix} + \begin{bmatrix} \mathbf{K}_{uu} & \mathbf{K}_{u\phi} & \mathbf{K}_{u\theta} \\ \mathbf{K}_{\phi u} & \mathbf{K}_{\phi\phi} & \mathbf{K}_{\phi\theta} \\ 0 & 0 & \mathbf{K}_{\theta\theta} \end{bmatrix}\begin{Bmatrix} \mathbf{u}_u^e \\ \mathbf{u}_\phi^e \\ \mathbf{u}_\theta^e \end{Bmatrix} = \begin{Bmatrix} \mathbf{F}_u - \mathbf{F}_{u\theta} \\ \mathbf{F}_\phi - \mathbf{F}_{\phi\theta} \\ \mathbf{F}_\theta - \mathbf{F}_{\theta\theta} \end{Bmatrix} \tag{37}$$

where the matrices $\mathbf{C}_{\theta u}$ and $\mathbf{C}_{\theta\phi}$ are damping matrices due to thermal-mechanical and thermal-electrical coupling effect, respectively and $\mathbf{C}_{\theta\theta}$ is damping matrix due to thermal field. The matrices $\mathbf{K}_{u\phi}$ and $\mathbf{K}_{\phi u}$ are stiffness matrices due to piezoelectric-mechanical coupling effect, and $\mathbf{K}_{u\theta}$ and $\mathbf{K}_{\phi\theta}$ are stiffness matrices due to thermal-mechanical and thermal- electrical coupling, respectively. The matrices $\mathbf{K}_{uu}$, $\mathbf{K}_{\phi\phi}$ and $\mathbf{K}_{\theta\theta}$ are stiffness matrices due to mechanical, electrical and thermal fields, respectively. The vectors

$\mathbf{F}_u, \mathbf{F}_\phi$ and $\mathbf{F}_\theta$ are force vectors due to mechanical, electrical and thermal fields, respectively and the force vectors $\mathbf{F}_{u\theta}$, $\mathbf{F}_{\phi\theta}$ and $\mathbf{F}_{\theta\theta}$ result from the higher order temperature field.

4. Numerical results and discussion

At first, the results from the higher order temperature theory (HOT) are compared with those obtained using a commercial finite element code ANSYS and a linear temperature field. To simplify the model for correlation, only 0° uniform fiber-reinforced Graphite/Epoxy laminate without actuators is considered, which implies that only thermal-mechanical coupling is presented in this case. The dimensions of the plate are such that $a = 0.2032$ m, $b = 0.1016$ m and $h = 0.01016$ m (Fig. 1). The plate is subjected to a heat flux of $q_t = 3000$ W/m^2 on top and it is insulated at the bottom. All four sides are maintained at room temperature (20°C). In the two-dimensional analysis using the current theory, the plate is discretized using ten elements along the plate length and four elements along the plate width. In the full three-dimensional finite element analysis using ANSYS, $10 \times 4 \times 6$ 8-node brick elements are used. The through-the-thickness temperature variation of the central point in the plate is shown in Fig. 3. The square symbol is used to denote the results based on the higher order temperature field, the circle data points are used to represent the results obtained using the linear temperature field and the triangular data points indicate the solution obtained from ANSYS. From Fig. 3, it is seen that the HOT solution is in very good agreement with that obtained using ANSYS. Since the bottom of the plate is insulated, the slope of the curve at $z = -h/2$ (bottom of the plate) is infinity ($\partial\theta/\partial z = 0$) which obviously satisfies the boundary condition (Eq. (16)) at the bottom surface. However, the linear

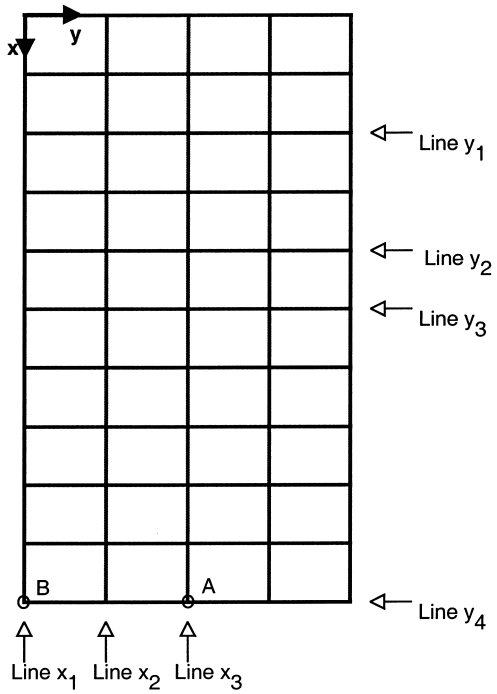

Fig. 2. 2-D Finite element model of the thermo-piezoelectric-mechanical theory.

temperature distribution deviates on top and bottom surfaces, which implies that it cannot satisfy the thermal boundary conditions on the plate surfaces.

Further correlations of the temperature distributions along plate length and width (lines x_1, x_2, x_3 and y_1, y_2, y_3, y_4, Fig. 2), between HOT and ANSYS, are presented in Figs. 4 and 5. It must be noted that curve fitting is used in presenting these distributions. Fig. 4 shows the temperature distributions in mid-plane along x-axis for line x_2 and x_3. As seen, the solutions from the higher order temperature theory agree very well with ANSYS. The magnitude of temperature rise along the central line x_3 is larger than that along x_2. This is because line x_2 is closer to the boundary that is maintained at room temperature. The temperature rise in the plate is a result of the heat flow from the top surface to the side boundaries where heat finally dissipates.

The temperature rise is maximum at the center of the plate and has the smallest values near the plate side boundaries. The temperature distribution is also symmetric since the geometry of the plate, the thermal boundary conditions and the external loading are all symmetric. The temperature distributions in mid-plane along the plate width (y-axis, Fig. 2) are shown in Fig. 5. There is excellent agreement between the results from HOT and ANSYS for both lines y_1 and y_3. Since line y_1 is closer to the boundary, which is maintained at room temperature, the magnitudes of temperature rise along this line are smaller compared to those along line y_3.

From the results presented in Figs. 3–5, it is clear that the higher order temperature field is very effective in accurately predicting the temperature distributions throughout the plate. It is important to note that HOT is a two-dimensional theory implemented using plate type finite element. However, the results are comparable to those obtained using the three-dimensional ANSYS model. Therefore, the present theory provides a framework which is both accurate and computationally efficient.

Next, comparisons are made between the plate deflections obtained using HOT and ANSYS. The deflections along plate length due to the temperature field are presented in Fig. 6 and excellent agreement is observed between HOT and ANSYS. The maximum absolute value of deflection occurs at plate tip, as expected. A convex distribution is observed along line x_3. This is due to the expansion of the structure caused by thermal loading.

Fig. 7 presents a comparison of the deflection variation along plate width (y-axis, Fig. 2). Again, the solutions from HOT and those obtained using ANSYS agree very well. The deflections along all three lines (y_1, y_2 and y_3, Fig. 2) are symmetric. The deflections also reach their peak values at the plate

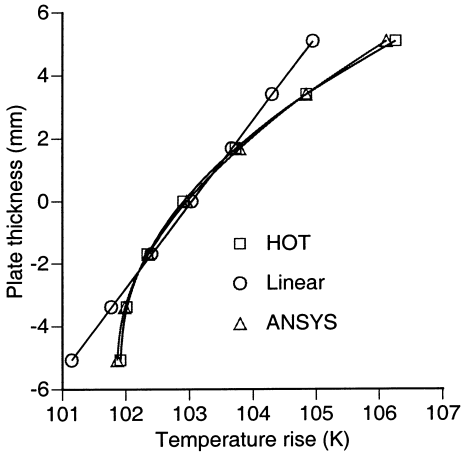

Fig. 3. Correlation; temperature variation through plate thickness.

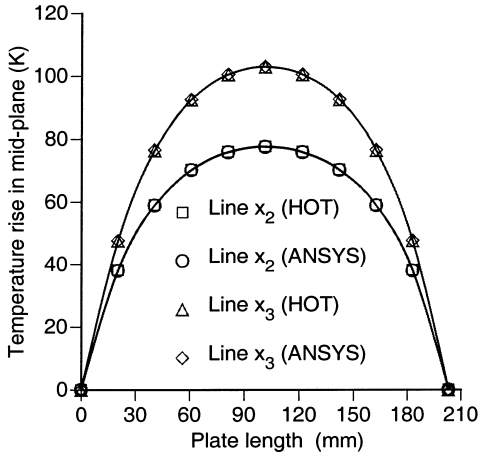

Fig. 4. Correlation; temperature variation along plate length.

center. Since line y_1 is closer to the fixed edge, it is more affected by the fixed boundary condition. The curvature of deformation along line y_1 is thus smaller compared to those along line y_2 and y_3. The maximum positive deflection occurs at the center of line y_2, because the temperature variation here is larger and it is far from the fixed edge (compared to line y_1). Since line y_4 is located farthest from the fixed boundary, the curvature of deformation is the largest in this case due to the least effects from the fixed boundary.

The effect of stacking sequence on the temperature field is shown in Fig. 8. It is observed that, under the same thermal loading condition, the peak values from the three stacking sequences are different. The peak value is the maximum when the stacking sequence is $[0^\circ/0^\circ/0^\circ/0^\circ]$s, it is minimum when the stacking sequence is $[90^\circ/90^\circ/90^\circ/90^\circ]$s and the peak value for the stacking sequence $[0^\circ/90^\circ/0^\circ/90^\circ]$s is somewhere in between. The reason for this is that composite material has different thermal conductivity coefficients along fiber and across fiber (see Table 1). For the composite material discussed here (Graphite/Epoxy), the thermal conductivity along fiber ($\kappa_{11} = 4.48$) is larger than the thermal

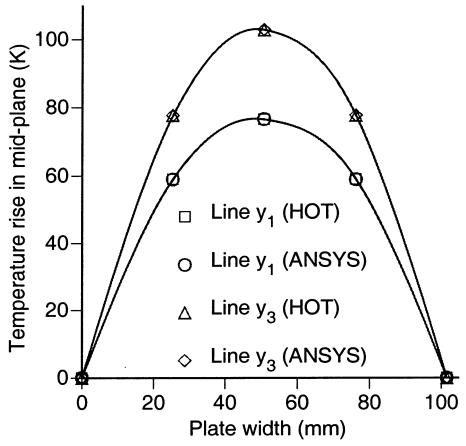

Fig. 5. Correlation; temperature variation along plate width.

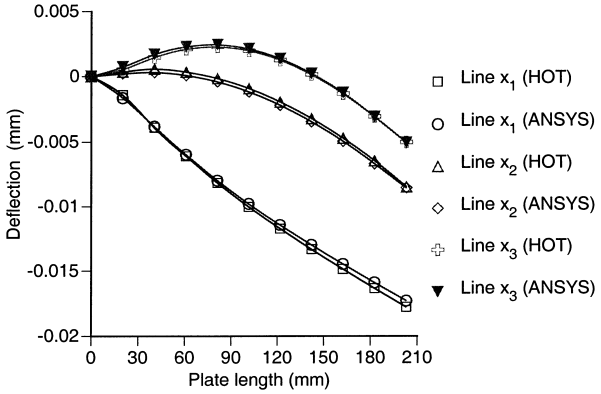

Fig. 6. Correlation; deflection along plate length.

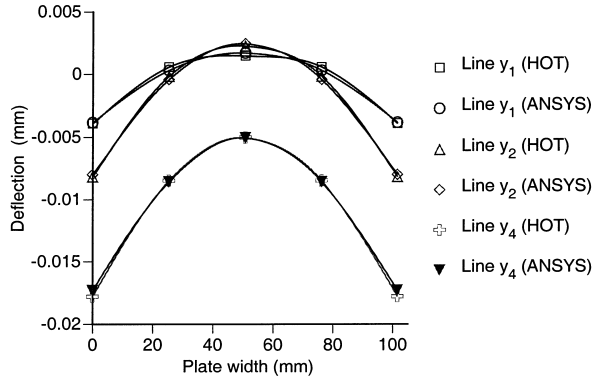

Fig. 7. Correlation; deflection along plate width.

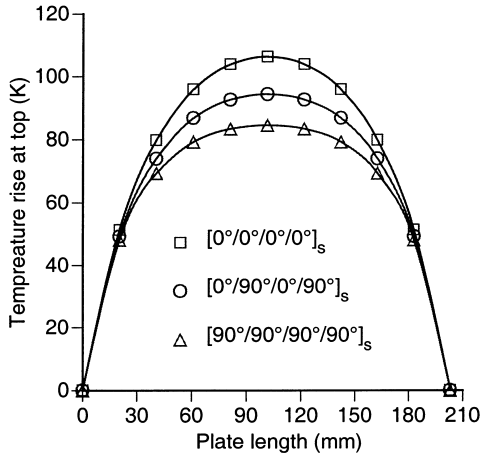

Fig. 8. Effect of stacking sequence on temperature variation.

conductivity across fiber ($\kappa_{22} = 3.21$). In the case of the [90°/90°/90°/90°]s stacking sequence, the larger thermal conductivity coefficient is along width coordinate (the short side, Fig. 2), therefore heat is transmitted easily to the surroundings thereby reducing the temperature variation.

The effect of stacking sequence on plate deflection, along length and width directions, is shown in Figs. 9 and 10, respectively. From Fig. 9, the maximum absolute value of tip deflection is obtained with the [90°/90°/90°/90°]s laminate. This is because, in this case, the Young's modulus along fiber ($E_1 =$ 144.23 Gpa) is along width coordinate and the Young's modulus across fiber ($E_2 = 9.65$ GPa) is along length coordinate. This makes the plate soft in length direction resulting in much larger deflection compared to the case of [0°/90°/0°/90°]s and [0°/0°/0°/0°]s stacking sequences (Fig. 9). The opposite trend is observed in Fig. 10 since the [90°/90°/90°/90°]s is stiff along width direction. Since the Young's modulus along x-axis (Fig. 2) for [0°/90°/0°/90°]s is larger than that for [90°/90°/90°/90°]s and smaller than that for [0°/0°/0°/0°]s, the deflection in this case falls between the other two cases (Figs. 9 and 10).

The difference between the two models, the newly developed thermo-piezoelectric-mechanical (''coupled'') model and the standard (''uncoupled'') model, with one-way coupling between the three fields, is investigated next.The same composite plate structure subjected to the same thermal load is used. Piezoelectric actuators are surface bonded to top and bottom surfaces of the plate (Fig. 1). The actuator dimensions are such that length = 0.08128 m, width = 0.0508 m and height = 0.00254 m. A

Table 1
Material properties of PZT and Graphite/Epoxy composite

	PZT	Graphite/Epoxy
Elastic Moduli (GPa):		
E_{11}	63	144.23
E_{22}	63	9.65
E_{33}	63	9.65
Shear Moduli (GPa):		
G_{23}	24.6	3.45
G_{13}	24.6	4.14
G_{12}	24.6	4.14
Poisson's Ratio:		
ν	0.28	0.3
Coefficients of Thermal Expansion (μm/m-°C):		
α_{11}	0.9	1.1
α_{22}	0.9	25.2
Density (kg/m^3):		
ρ	7600	1389.23
Piezoelectric Charge Constant (pm/V):		
$e_{31} = e_{32}$	150	–
Electric Permittivity (nf/m):		
$b_{11} = b_{22}$	15.3	–
b_{33}	15.0	–
Pyroelectric Constant (μC/m^2-°C)		
d_3	20	–
Thermal Conductivity (W/m-°C):		
κ_{11}	2.1	4.48
κ_{22}	2.1	3.21
Heat Capacity (J/kg-°C):		
c_E	420	1409
Curie Temperature (°C)		
T_c	365	–

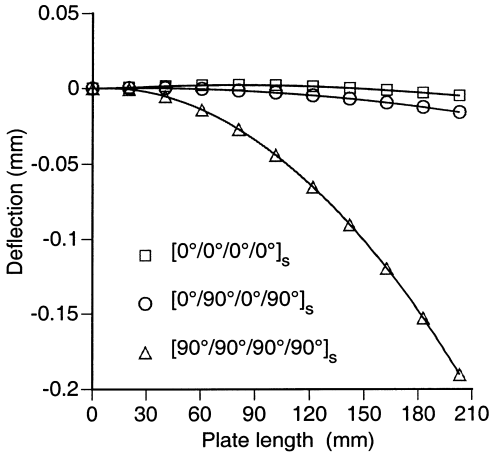

Fig. 9. Effect of stacking sequence on deflection along plate length.

comparison of the plate deflection, obtained using the coupled and the uncoupled model, is presented in Fig. 11. It can be seen that under thermal loads, the deflection from the coupled model is smaller compared to that obtained using the uncoupled model. This is due to the interaction between thermal, piezoelectric and displacement fields in the coupled model. The coupled model considers thermoelectric effect, which implies that thermal energy can be stored in the form of electrical energy. Therefore, thermally induced deflection is reduced. Fig. 12 shows that the plate deflection is reduced by 11.5% at the plate tip (point A, Fig. 2).

It is also necessary to examine the effect of actuation, with the application of voltage, on the two models. The same example structural configuration and thermal loading condition are used. Fig. 13 shows the actuation effect on the deflection of the plate along line x_3 (Fig. 2) with voltages applied on the actuators. The case of 0 V implies that only thermal load is considered. The application of a voltage implies that both thermal load and piezoelectric actuation are present. As observed before, the magnitude of plate deflection, predicted by the uncoupled theory, is larger compared to that predicted

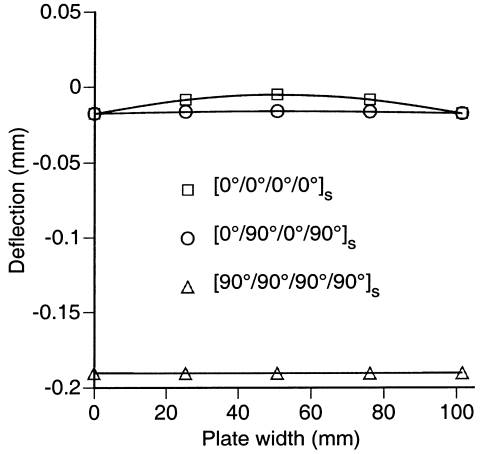

Fig. 10. Effect of stacking sequence on deflection along plate width.

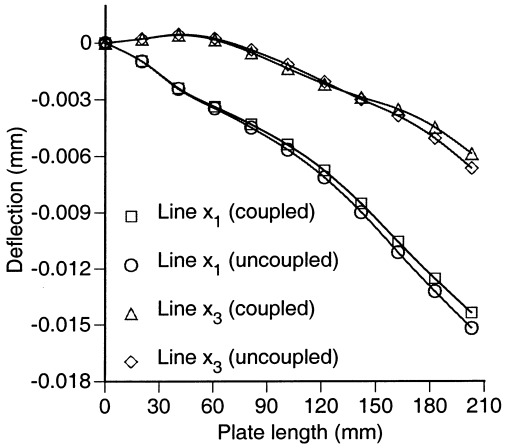

Fig. 11. Coupling effect on deflection along plate length.

by the coupled theory since more transformation of mechanical energy into thermal and electrical energies due to coupling effects is considered in the coupled model. The difference between the two theories is due to the fact that the uncoupled theory neglects both piezoelectric effect of actuation and thermal coupling effect due to thermal loads. The difference is smaller in the absence of external voltage (0 V), compared to the 200 V case. This is due to the presence of additional piezoelectric-mechanical coupling effect in the latter case. Fig. 14 presents a comparison of the control authority which is defined as the reduction in plate deflection with actuation. Compared to the coupled model, the reduction in plate deflection at point B (Fig. 2) is overpredicted significantly (17.5 percent) by the uncoupled theory.

5. Conclusion

A higher order temperature (HOT) field theory is developed to accurately model the temperature distribution in laminated structures. The theory is capable of satisfying all thermal surface boundary

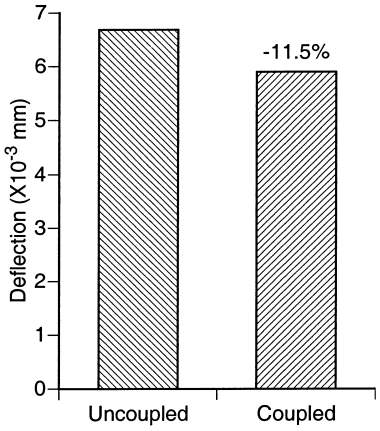

Fig. 12. Comparison of tip deflection, coupled and uncoupled theories.

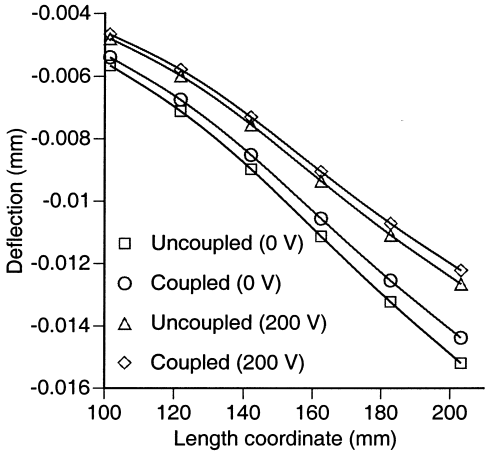

Fig. 13. Effect of actuation on deflection along plate length.

conditions. The temperature field is used in the development of a coupled thermo-piezoelectric-mechanical theory for the accurate analysis of smart composite structures. A refined third order displacement field is used to accurately capture the transverse shear effects. The mathematical model is implemented using finite element technique. The developed procedure is used to investigate the response of composite plates (one edge fixed and others free) with surface bonded piezoelectric actuators in the presence of thermal loads. The results of the coupled theory are also compared with those obtained using the conventional uncoupled theory. The following important observations are made from the present study.

1. Excellent agreement is observed in the temperature distribution throughout the laminate between the higher order temperature field and the general-purpose finite element code ANSYS. The HOT satisfies all thermal boundary conditions.
2. The plate deflections predicted by HOT also agree very well with ANSYS.
3. Stacking sequence of the primary structure affects both temperature field and displacement field due to orthotropic material properties and changes in thermal conductivity across and along fiber

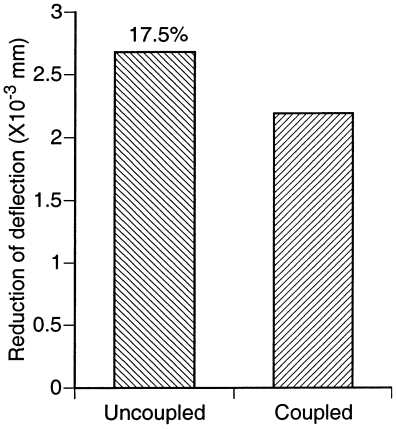

Fig. 14. Comparison of control authority due to actuation, coupled and uncoupled theories.

directions.

4. The deflection predicted by the coupled theory is always smaller, compared to the coupled theory, due to the transformation of mechanical energy into thermal and electrical energy in the coupled model.
5. The uncoupled theory overpredicts control authority significantly.

Acknowledgements

The research is supported by Air Force Office of Scientific Research, grant number F49620-96-0195, technical monitor Dr. Brian Sanders.

References

Crawley, E.F., 1994. Intelligent Structures for Aerospace: A Technology Overview and Assessment. AIAA Journal 32 (8), 1689–1699.

Chopra, I., 1996. Review of Current Status of Smart Structures and Integrated Systems. SPIE 2717, 20–62.

Mitchell, J.A., Reddy, J.N., 1995. A Refined Hybrid Plate Theory for Composite Laminates with Piezoelectric Laminae. International Journal of Solids Structure 32 (16), 2345–2367.

Tauchert, T.R., 1992. Piezothermoelastic Behavior of a Laminated Plate. Journal of Thermal Stresses 15 (1), 25–37.

Lee, H., Saravanos, D.A., 1996. The Effect of Temperature Induced Material Property Variations on Piezoelectric Composite Plates. In: Proceedings of the AIAA/ASME/ASCE/AHS/ASC 37th Structures, Structural Dynamics and Materials Conference, AIAA, Salt Lake City, UT, 1781–1788.

Lee, H., Saravanos, D.A., 1997. Active Compensation of Thermally Induced Bending and Twisting in Piezoceramic Composite Plates. In: Proceedings of the AIAA/ASME/ASCE/AHS/ASC 38th Structures, Structural Dynamics and Materials Conference, AIAA, Kissimmee, FL, 120–130.

Chattopadhyay, A., Li, J. and Gu, H., (in press). A Coupled Thermo-Piezoelectric-Mechanical Model for Smart Composite Laminates. In: Proceedings of the 39th AIAA/ASME/ASCE/AHS/ASC/SDM Conference and AIAA/ASME Adaptive Structures Forum, AIAA, Long Beach, CA, 1998, pp. 2891–2901 (AIAA Journal, in press).